MLLT6 maintains *PD-L1* expression and mediates tumor immune resistance

Sandeep Sreevalsan[1], Marietta Döring[1], Maciej Paszkowski-Rogacz[2] (iD), Melanie Brux[1], Carolina Blanck[2], Marten Meyer[3], Frank Momburg[3], Frank Buchholz[1,2] (iD) & Mirko Theis[1,2,*] (iD)

Abstract

Tumor cells subvert immune surveillance by harnessing signals from immune checkpoints to acquire immune resistance. The protein PD-L1 is an important component in this process, and inhibition of PD-L1 elicits durable anti-tumor responses in a broad spectrum of cancers. However, immune checkpoint inhibition that target known pathways is not universally effective. A better understanding of the genetic repertoire underlying these processes is necessary to expand our knowledge in tumor immunity and to facilitate identification of alternative targets. Here, we present a CRISPR/Cas9 screen in human cancer cells to identify genes that confer tumors with the ability to evade the cytotoxic effects of the immune system. We show that the transcriptional regulator MLLT6 (AF17) is required for efficient PD-L1 protein expression and cell surface presentation in cancer cells. MLLT6 depletion alleviates suppression of CD8^{+} cytotoxic T cell-mediated cytolysis. Furthermore, cancer cells lacking *MLLT6* exhibit impaired STAT1 signaling and are insensitive to interferon-γ-induced stimulation of *IDO1*, *GBP5*, *CD74*, and MHC class II genes. Collectively, our findings establish MLLT6 as a regulator of oncogenic and interferon-γ-associated immune resistance.

Introduction

Tumor cells evade immune destruction by exploiting immune-modulatory pathways such as immune checkpoints (Ribas & Wolchok, 2018) that are responsible for maintaining peripheral tolerance under physiological conditions (Chen & Mellman, 2013). The interaction between the proteins, programmed cell death 1 (PD-1) expressed on T lymphocytes, and programmed cell death 1 ligand 1 (PD-L1) on tumor cells inhibits the effector function of antigen-specific CD8^{+} cytotoxic T cells (CTLs) and is an integral part of an important immune checkpoint (Sun *et al*, 2018). Therapeutic blockade of the PD-1-PD-L1 interaction has led to unprecedented response rates in patients with different tumors and has brought about a new class of cancer therapy (Ribas & Wolchok, 2018). PD-L1 (CD274) expression levels and T cell infiltration in tumor tissues are established prognostic markers and are predictive of the efficacy of checkpoint inhibition therapy (Sun *et al*, 2018; Havel *et al*, 2019). Nevertheless, many tumors fulfilling these criteria exhibit primary resistance to therapy (Sharma *et al*, 2017) or patients who initially respond subsequently relapse despite continuous treatment (Sharma *et al*, 2017). Oncogenic mechanisms in tumor cells, for instance, amplification of the *PD-L1* genomic locus (Green *et al*, 2010) or mutations in genes such as *PTEN* (Parsa *et al*, 2007), *TP53* (Wieser *et al*, 2018), *MYC* (Casey *et al*, 2016), or *JAK/STAT* (Ikeda *et al*, 2016) alter *PD-L1* expression levels and confer immune resistance. In addition, inflammatory cytokines such as interferon-γ (IFN-γ), often present in the tumor microenvironment, stimulate *PD-L1* expression (Ni & Lu, 2018) in concert with other immune-related genes, e.g. *IDO1* (Gomes *et al*, 2018), to grant tumor cells an escape from immune attack (Gomes *et al*, 2018). Besides these pro-tumorigenic effects of IFN-γ, anti-tumorigenic activities have been reported such as upregulation of MHC class I molecules (Seliger *et al*, 2008) or induction of chemokines leading to increased recruitment of CTLs to the tumor mass (Kunz *et al*, 1999). Therefore, a better understanding of the immune-inhibitory mechanisms that are prevalent in individual tumor types and a deeper knowledge of *PD-L1* regulation and IFN-γ signaling may facilitate improved tumor stratification and assist in optimizing immune checkpoint therapy.

Loss-of-function genetic screens utilizing the CRISPR/Cas9 system have been successfully employed to study genotype–immunophenotype correlations and to identify novel molecules that affect immune resistance (Zhu *et al*, 2016; Burr *et al*, 2017; Manguso *et al*, 2017; Mezzadra *et al*, 2017; Patel *et al*, 2017). However, our knowledge of the genetic repertoire modulating the PD-1–PD-L1 immune checkpoint is still incomplete. Therefore, we set up a CRISPR/Cas9 loss-of-function screen to identify and characterize additional genes implicated in cancer immune resistance and *PD-L1* regulation.

1   National Center for Tumor Diseases (NCT/UCC) Dresden, German Cancer Research Center (DKFZ), University Hospital Carl Gustav Carus, Technische Universität Dresden, Helmholtz-Zentrum Dresden-Rossendorf (HZDR), Dresden, Germany
2   Medical Systems Biology, Medical Faculty Carl Gustav Carus, Technische Universität Dresden, Dresden, Germany
3   Antigen Presentation & T/NK Cell Activation Group, Clinical Cooperation Unit 'Applied Tumor Immunity', German Cancer Research Center (DKFZ), Heidelberg, Germany
    *Corresponding author. Tel: +49 351 46340277; E-mail: mirko.theis@nct-dresden.de

Results

CRISPR/Cas9 screen identifies regulators of *PD-L1*

To identify new regulators of both oncogenic and immune-associated *PD-L1* expression, we performed pooled genetic screens in the absence and presence of IFN-γ, respectively, utilizing an sgRNA library targeting 1,572 human genes (Dataset EV1). To select a suitable cell line for the screens, we analyzed *PD-L1* transcript levels in 675 different cancer cell lines (Klijn *et al*, 2015) and chose the human colon carcinoma cell line RKO owing to its high expression levels of *PD-L1* (Dataset EV2, Fig EV1A). In order to monitor *PD-L1* expression in RKO cells, we generated a reporter line by knocking in *eGFP* into the endogenous *PD-L1* genomic locus (Fig EV1B). Precise tagging was confirmed by sequencing the insertion site, which revealed an *eGFP* tagged *PD-L1* gene (Fig EV1C). To rule out that the eGFP-tag interferes with the localization of the PD-L1 protein, we performed immunofluorescence microscopy and observed that the PD-L1-eGFP fusion protein localizes at the plasma membrane (Fig EV1D). Furthermore, to ensure that *PD-L1* expression can be stimulated, we treated the cells with increasing doses of IFN-γ. We observed a dose-dependent induction of PD-L1-eGFP by IFN-γ with an EC_{50} of 600 pg/ml (Fig EV1E and F), demonstrating the suitability of the reporter cell line for screening oncogenic and immune-associated *PD-L1* expression.

Both screens (with and without IFN-γ, Fig 1A) were performed by transducing the reporter cells with the lentiviral sgRNA library (Dataset EV1, Fig 1A) and enriching PD-L1-eGFP^{low} cells to > 99.8% purity by FACS (Fig EV2). Sequencing the sgRNAs expressed in the PD-L1-eGFP^{low} cells revealed that the positive controls targeting the genes *PD-L1* ($\log_2$ fold = 1.2–6.3) or *eGFP* ($\log_2$ fold = 6.2–9.6) (Dataset EV3) were among the most substantially enriched sgRNAs in both screens (Fig 1B). Notably, multiple gRNAs targeting the positive control genes *PD-L1* and *eGFP* were enriched. In contrast, we did not observe enrichment of more than one gRNA for any other gene. Strikingly, an sgRNA targeting the *signal transducer and activator of transcription 1* (*STAT1*), a well-characterized mediator of IFN-γ signaling upstream of *PD-L1* (Garcia-Diaz *et al*, 2017), was enriched in the presence of IFN-γ ($\log_2$ fold = 4.7) but not in its absence ($\log_2$ fold = −3.4; Fig 1B, Dataset EV3). These results corroborate the potential of the screening setup to identify genes modulating *PD-L1* expression via the oncogenic or immune-associated pathway.

To monitor the screening procedure and identify genes implicated in basic cellular processes such as cell growth and division, we spiked control sgRNAs into the initial library, targeting essential, and non-essential genes (Evers *et al*, 2016). The sgRNA library composition was analyzed after culturing cells but without sorting for cells based on *PD-L1* expression. We observed that 44 (97.8%) out of 45 essential genes were depleted by more than two-fold ($\log_2$ fold < −1) (Fig 1C), whereas 37 (78.7%) out of 47 non-essential genes were unaltered or mildly changed ($\log_2$ fold > −1 and < 1) (Fig 1C, Dataset EV3). Strikingly, both PD-L1 screens (with and without IFN-γ) identified the gene *MLLT6* ($\log_2$ fold = 4.4 (−IFN-γ), 6.6 (+IFN-γ)) (Fig 1B) as required for efficient *PD-L1* expression. Notably, *MLLT6* did not score in the viability screen ($\log_2$ fold = −0.1; Fig 1C) in accordance with findings of Zhang *et al* (2010). In summary, the screen identified

MLLT6 as a putative regulator of *PD-L1* that is not essential for cell growth and division.

MLLT6 is required for *PD-L1* expression

Myeloid/lymphoid or mixed-lineage leukemia translocated to 6 (*MLLT6*, also referred to as *AF17*) encodes a 112 kDa protein that has been reported to exhibit transcriptional regulator activity (Prasad *et al*, 1994; Saha *et al*, 1995). Analyzing the Cancer Cell Line Encyclopedia (CCLE) transcriptome database revealed that *MLLT6* is widely expressed in diverse cancer types (Fig EV3A). Interestingly, a dataset from Szasz *et al*, 2016 shows a statistically significant correlation (P = 4.7e-6) between poor overall survival of patients with gastric cancer and high expression levels of *MLLT6* (Fig EV3B). Strikingly, the prognostic power of *MLLT6* was comparable to that of *HER-2* (P = 6.7e-5) (Szasz *et al*, 2016), a well-established biomarker in several types of cancers, including gastric cancer (Boku, 2014; Fig EV3B).

To validate MLLT6 as a regulator of *PD-L1* and to exclude possible effects of tagging PD-L1 with eGFP in the reporter line, we depleted MLLT6 by CRISPR/Cas9-mediated genome editing in RKO wild-type cells. After confirming successful *MLLT6* knockout in a monoclonal cell line (Appendix Fig S1B) and MLLT6 mRNA depletion (Fig EV4D), we measured *PD-L1* expression by flow cytometry and detected a significant decrease (P < 0.01, MFI MLLT6 KO = 397, MFI control = 423) in PD-L1 abundance on the cell surface (Fig 2A). To confirm these findings in a cancer type other than colon carcinoma (RKO), we generated polyclonal *MLLT6* knockout cells of the human osteosarcoma cell line U2OS (Appendix Fig S1C), the cervical carcinoma cell line HeLa (Appendix Fig S2A and B), and the colon carcinoma cell line SW480 (Appendix Fig S2D and E). As observed in RKO cells, flow cytometry analysis revealed a significant decrease in the number of cells with high PD-L1 surface presentation in the U2OS (Fig 2B) and HeLa (Appendix Fig S2C) knockout cells but not in SW480 (Appendix Fig S2F). Hence, efficient PD-L1 surface presentation depends on *MLLT6* in diverse cell lines from different cancer types.

To exclude possible Cas9 off-target effects, we investigated if PD-L1 surface presentation can be restored by exogenous expression of LAP-tagged (Poser *et al*, 2008) *MLLT6* encoded on a bacterial artificial chromosome (BAC) in an *MLLT6* knockout line (Appendix Fig S3A). Correct localization and expression of MLLT6-LAP fusion protein was confirmed by immunofluorescence (Appendix Fig S3B), and we observed that PD-L1 surface presentation was largely restored in the *MLLT6* knockout lines (Fig 2B, MFI control = 369, MFI MLLT6 KO = 290, MFI MLLT6 KO + BAC = 313). Therefore, MLLT6-LAP expression can substitute for endogenously encoded MLLT6, rescuing the loss-of-function phenotype and validating the functional importance of *MLLT6* on PD-L1 plasma membrane expression.

These results prompted us to investigate whether the loss of PD-L1 cell surface expression after *MLLT6* knockout is a result of reduced cellular levels. Quantification of total cellular PD-L1 by immunoblotting revealed a significant reduction in the levels of PD-L1 in multiple monoclonal *MLLT6* knockout lines in RKO cells (Figs 2C and EV4A–C), and this phenotype was rescued by MLLT6-LAP expression (Fig 2C). To exclude sgRNA dependent
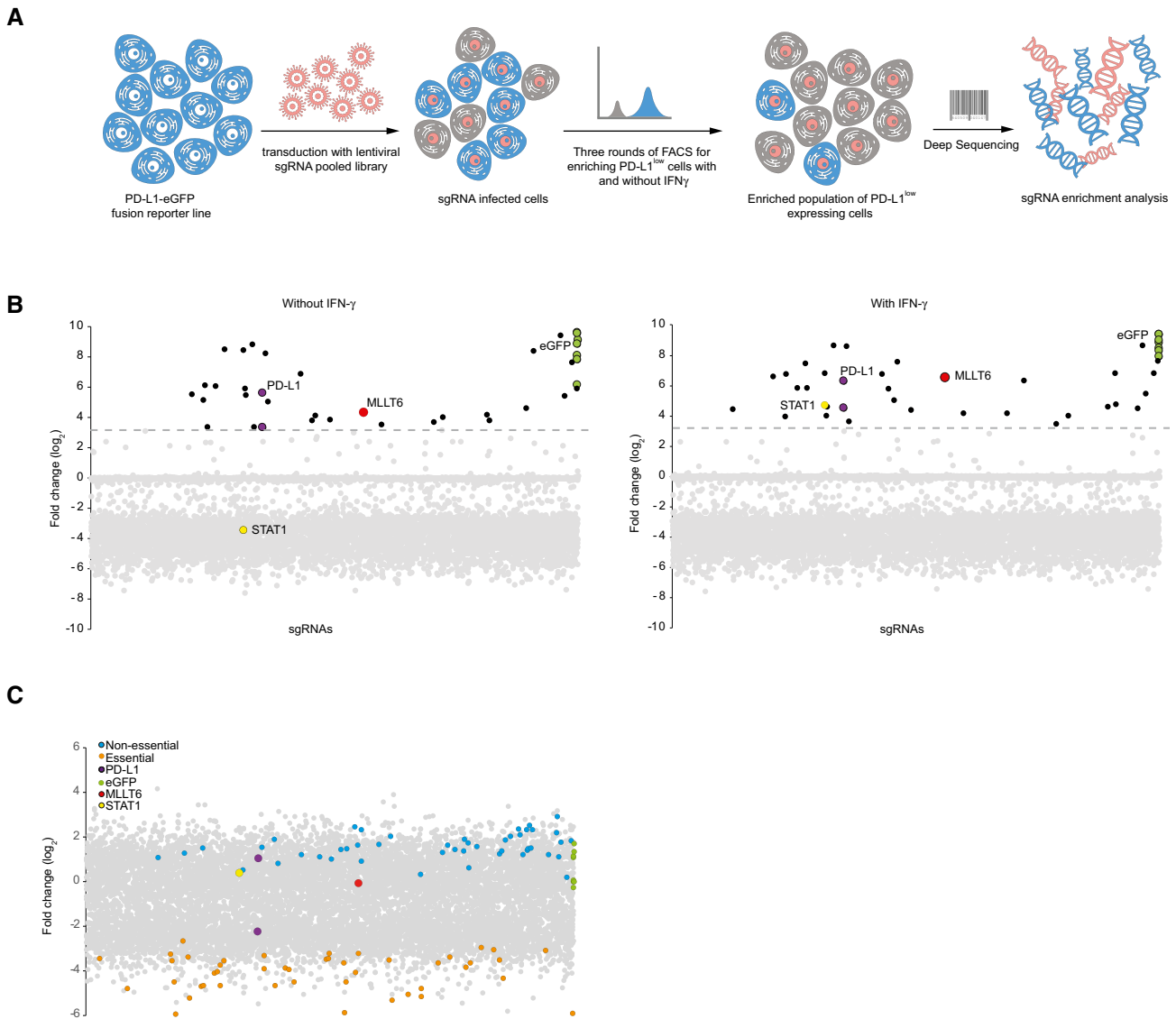
Figure 1. CRISPR screen identifies *MLLT6* as a regulator of *PD-L1*.

A Schematic of the screen for *PD-L1* regulators in the presence and absence of IFN-γ. RKO reporter cells expressing PD-L1-eGFP fusion protein (blue) were mutagenized with an sgRNA/Cas9 library. PD-L1^{low} cells were enriched by FACS, and sgRNA target genes were identified by deep sequencing. An enrichment analysis determined frequencies of different sgRNAs and their target genes.

B sgRNA frequencies (log$_2$ of fold change) in PD-L1^{low} cells unstimulated (left) or IFN-γ stimulated (right). Enriched sgRNAs (dashed line) are highlighted; hit genes (black, red) and controls (green, yellow or purple) are shown and labeled with target gene names.

C sgRNA frequencies (log$_2$ of fold change) in viability screen. sgRNAs targeting controls are highlighted; essential (orange), non-essential (blue). Genes attributed to *PD-L1* modulation are shown in different colors (red, yellow and purple).

effects, we repeated this experiment with three additional sgRNAs targeting different sites of the *MLLT6* genomic locus (Appendix Fig S4). All sgRNAs reduced *MLLT6* mRNA expression (Appendix Fig S4A) and concomitantly reduced PD-L1 expression levels (Appendix Fig S4B).

To investigate whether *MLLT6*-dependent PD-L1 protein expression is associated with *PD-L1* transcription, we performed qRT–PCR and observed a 42% reduction in *PD-L1* mRNA levels in U2OS *MLLT6* knockout cells (Fig 2D). Similarly, *MLLT6* knockout in RKO

cells showed reduction in *PD-L1* mRNA levels and MLLT6-LAP expression replenished the levels of PD-L1 (Fig EV4D). These results imply that the reduced PD-L1 level in MLLT6-depleted cells is at least, in part, due to transcriptional regulation of the *PD-L1* gene by MLLT6.

MLLT6 also scored as a hit in the screen where cells were treated with IFN-γ to modulate *PD-L1* expression (Fig 1B). To investigate the role of *MLLT6* in IFN-γ-stimulated expression of *PD-L1*, we analyzed the cell surface expression of PD-L1
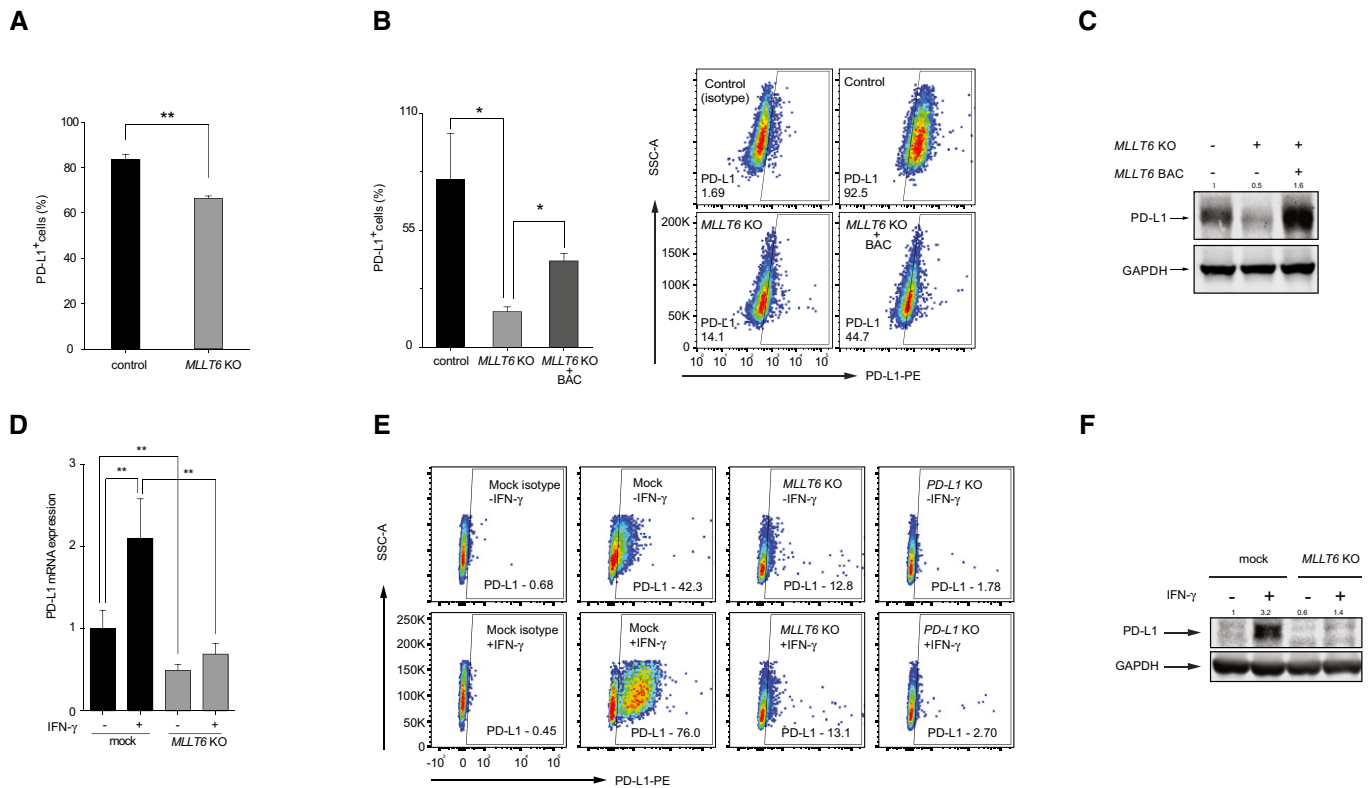
Figure 2. MLLT6 regulates expression of PD-L1.

A PD-L1 cell surface presentation (percentage ± SD) in RKO mock control (black) or monoclonal MLLT6 knockout cells (gray) (Student's t-test; **P < 0.01; n = 3 biological replicates; degrees of freedom (df) = 2).

B MLLT6 BAC mediated rescue in U2OS cells (left) showing percentage ± SD of PD-L1 cell surface presentation in mock control (black), MLLT6 polyclonal knockout (light gray) and MLLT6 knockout + BAC cells (dark gray) (Student's t-test; *P < 0.05; n = 3 biological replicates; df = 2). Representative flow cytometry plots (right) of PD-L1 cell surface presentation after staining with anti-PD-L1 antibody (top right, bottom left, bottom right) and isotype control (top left). Percentages of cells in the PD-L1+ gate as indicated.

C Total cellular protein levels of PD-L1 (top) and GAPDH (bottom) in monoclonal RKO MLLT6 knockout, mock control or MLLT6 knockout + BAC cells visualized by immunoblotting. Numbers indicate relative band intensities of PD-L1 protein normalized to GAPDH.

D PD-L1 transcript levels in U2OS mock (black) and polyclonal MLLT6 knockout lines (gray) treated with and without IFN-γ normalized to expression in mock U2OS cells without IFN-γ treatment (ANOVA; **P < 0.01; n = 4 biological replicates; df = 12).

E Representative flow cytometry plots of PD-L1 cell surface presentation in the presence and absence of IFN-γ in mock, polyclonal MLLT6 knockout and PD-L1 knockout cells. Percentages of cells in the PD-L1+ gate after staining with anti-PD-L1 antibody or isotype control as indicated.

F Total cellular protein levels of PD-L1 (top) and GAPDH (bottom) in U2OS polyclonal MLLT6 knockout or mock control cells with and without IFN-γ stimulation. Numbers indicate relative band intensities of PD-L1 protein normalized to GAPDH.

Source data are available online for this figure.

protein. In control cells, we observed PD-L1 cell surface expression induced by IFN-γ (76.0%, Fig 2E) in agreement with previous findings (Garcia-Diaz et al, 2017). In contrast, we observed a strongly reduced sensitivity to IFN-γ in MLLT6 knockout cells (13.1%) (Fig 2E). To further characterize the role of MLLT6 on the immune-associated induction of PD-L1, we analyzed protein and mRNA expression upon IFN-γ treatment. We observed PD-L1 protein and transcript levels induced by IFN-γ in control cells (Fig 2D and F). However, no upregulation of PD-L1 was observed in MLLT6 knockout cells upon IFN-γ stimulation (Fig 2D and F). Taken together, these findings establish MLLT6 as a modulator of oncogenic and IFN-γ-associated PD-L1 expression in colon and cervical carcinoma and osteosarcoma cells.

MLLT6 mediates tumor immune resistance

Tumors are often infiltrated with CD8+ cytotoxic T lymphocytes (CTLs) that present T cell receptors (TCRs) to recognize cancer antigens (Sharma et al, 2017). Inactivating these CTLs can be a prerequisite for neoplasms to grow to full malignancy (Sharma et al, 2017) and is a hallmark of immune resistance (Sun et al, 2018). To investigate whether the depletion of MLLT6 changes the susceptibility of tumor cells to T cell-mediated cytolysis, we measured cell survival of knockout and control cells in the presence of CTLs and an anti-EpCAM-CD3 bi-specific T cell engager (EpCAM-CD3 BiTE) (Fig 3A). We first compared the cell surface presentation of EpCAM antigen on MLLT6 knockout and control U2OS cells and observed increased levels of EpCAM surface expression in cells devoid of MLLT6

(Appendix Fig S5). Next, CD8$^+$ T cells were isolated from human blood and activated using CD3/CD28 beads followed by assessing the CD8$^+$ T cell purity and activation status. We achieved > 96% CD8$^+$ T cell purity (Appendix Fig S6A) and confirmed expression of activation markers on more than 91% of the cells (Appendix Fig S6B). *MLLT6* knockout and control cells were mixed and cocultured in the presence or absence of activated T cells and varying amounts of EpCAM-CD3 BiTE. Strikingly, we found that *MLLT6* knockout cell numbers were significantly reduced in comparison with control cells (Fig 3B) when treated with increasing doses of EpCAM-CD3 BiTE (0.25, 0.5, 1 μg/ml) (Fig 3B). Furthermore, no reduction in knockout or control cell numbers was observed in the presence of the BiTE or activated T cells alone (Fig 3B), excluding non-specific effects. This finding indicates that *MLLT6* expression in tumor cells is necessary for suppression of CTL-mediated cytolysis and for maintenance of immune resistance.

To measure the kinetics of T cell-mediated tumor cell lysis, we stably integrated *eGFP* and *mCherry* reporter genes in control and *MLLT6* knockout cells, respectively, and followed cell survival by fluorescence time-lapse microscopy after coculturing equal proportions of control and *MLLT6* knockout cells with T cells and EpCAM-CD3 BiTE. As before, we observed no change in tumor cell survival comparing *MLLT6* knockout and control cells when treated with CTLs only (Appendix Fig S6C). In contrast, a significant difference (P = 5.5e-31) between *MLLT6* knockout and control cell numbers was observed when treated with both CTLs and BiTE (Fig 3C, Movie EV1). Differences in cell numbers started to be apparent five hours after addition of T cells and EpCAM-CD3 BiTE to tumor cells and progressed until 9.5 h where the number of *MLLT6* knockout cells was reduced to 30% compared to control cells (65%, Fig 3C, Movie EV1).

To exclude effects that can be attributed to the BiTE technology or the target epitope, we investigated cytotoxicity of CTLs employing bi-specific antibodies that recognize epidermal growth factor receptor (EGFR) or Erb-B2 receptor tyrosine kinase 2 (HER-2) and CD3. We first measured cell surface presentation of both receptors in *MLLT6* knockout and control cells and found HER-2 expression unaltered but EGFR expression increased in cells devoid of MLLT6 (Appendix Fig S5). We then treated *MLLT6* knockout cells with HER-2-CD3 or EGFR-CD3 bi-specific antibodies and CTLs and measured cell viability. Both bi-specific antibodies showed a significant reduction (P < 0.01) in *MLLT6* knockout cell numbers compared to controls (Fig 3D), corroborating results generated with the BiTE.

The observation that MLLT6 depletion leads to reduced PD-L1 levels (Fig 2) prompted us to compare *MLLT6* and *PD-L1* knockout cells in more detail. We engaged CTLs with *PD-L1* and *MLLT6* knockout cells employing bi-specific antibodies and followed cell survival. Strikingly, *MLLT6* knockout cells exhibited an increased vulnerability to CTL-mediated cytolysis compared to *PD-L1* knockout cells (Fig 3E). These results corroborate the efficacy of MLLT6 depletion on reducing tumor cell immune resistance and imply that other factors in addition to *PD-L1* regulation may be involved.

IFN-γ, a cytokine frequently present in the tumor microenvironment (Zaidi & Merlino, 2011), has been shown to induce the expression of *PD-L1* (Garcia-Diaz *et al*, 2017). To investigate the consequences of cytokine stimulation on immune resistance in *PD-L1* and *MLLT6* knockout cells, we examined T cell-mediated

cytotoxicity in the presence of IFN-γ. Interestingly, we observed that IFN-γ increases CTL-mediated cytolysis in *PD-L1* and *MLLT6* knockout cells in comparison with control cells (Fig 3E). In summary, these findings show that MLLT6 depletion alleviates the suppression of cytotoxic T cells in the presence and absence of IFN-γ.

IFN-γ signaling and *MLLT6*

The decreased sensitivity to IFN-γ in absence of MLLT6 (Fig 2) prompted us to hypothesize that *MLLT6* might play a role in IFN-γ signal transduction and that other genes in addition to *PD-L1* may be affected. To investigate this hypothesis, we systematically analyzed transcriptome changes after IFN-γ stimulation in *MLLT6* knockout and control cells by RNA-Seq. We first determined the transcriptome changes resulting from IFN-γ stimulation in U2OS cells and found 168 genes that showed at least a four-fold induction (FDR < 0.05; Fig 4A, Dataset EV4). As expected, a gene ontology enrichment analysis of these genes showed an association with IFN-γ processes (GO: 0034341; P = 1.911e-9; GO: 0060333; P = 5.542e-14; GO: 0071346; P = 7.167e-16; GO: 0019221; P = 4.280e-18) confirming our experimental setup. Interestingly, *MLLT6* transcript levels were unaltered after IFN-γ treatment ($\log_2$ fold = 0.28, FDR = 0.06), whereas *PD-L1* and *STAT1* were induced 3.6 (FDR = 0.002) and 7.7 fold (FDR = 3.1e-241), respectively (Fig 4A, Dataset EV4). Notably, the strongest induction was observed for transcripts of the genes *IDO1* ($\log_2$ fold = 12.2) and MHC class II molecules *CD74* ($\log_2$ fold = 13.9) and *HLA-DRA* ($\log_2$ fold = 13.5; Fig 4A, Dataset EV4).

Next, we investigated whether *MLLT6* knockout leads to changes in the cellular response to IFN-γ stimulation. Interestingly, 118 out of 168 transcripts were now insensitive to IFN-γ (Fig 4A, Dataset EV4, Appendix Fig S7), namely *PD-L1* ($\log_2$ fold = −1.0, FDR = 0.05), *STAT1* ($\log_2$ fold = −1.0, FDR = 1.6e-29), *CD74* ($\log_2$ fold = −7.9, FDR < 1.0e-100), and *IDO1* ($\log_2$ fold = −8.1, FDR = 2.0e-83). Remarkably, these genes where mildly reduced ($\log_2$ fold PD-L1 = −0.6; STAT1 = −0.9; IDO1 = −0.8) or even induced ($\log_2$ fold CD74 = 2.8) in *MLLT6* knockout cells without IFN-γ stimulation (Dataset EV4, Appendix Fig S8). Of note, *MLLT6* knockout reduced MHC class I gene expression in the presence of IFN-γ ($\log_2$ fold HLA-A = −0.6; HLA-B = −1.4; HLA-C = −0.2) but left it unaltered or induced in its absence ($\log_2$ fold HLA-A = 0.8; HLA-B = −0.3; HLA-C = 0.7) (Dataset EV4). However, the IFN-γ induced expression of the immunoproteasome components PSMB8 and PSMB9 were reduced in *MLLT6* knockout cells ($\log_2$ fold PSMB8 = −6.4, PSMB9 = −1.8) which might adversely affect MHC I peptide generation (Dataset EV4). In summary, these results present a set of genes that are insensitive to IFN-γ stimulation in cells lacking *MLLT6* expression.

To corroborate these findings, we nominated 86 genes from the list for validation by employing NanoString technology (Goytain & Ng, 2020). The NanoString technology quantifies gene expression by utilizing probes containing molecular barcodes that hybridize to transcripts, generating data comparable to qRT–PCR (Goytain & Ng, 2020). This dataset confirms the observations made from RNA-Seq and presents a gene set that changes significantly in the presence of IFN-γ in tumor cells devoid of *MLLT6* (Fig 4B, Dataset EV5). Strikingly, many genes in this set namely *HLA-DRA* (Matern *et al*, 2019), *HLA-DRB1* (Matern *et al*, 2019), *CD74* (Imaoka *et al*, 2019), *IDO1*
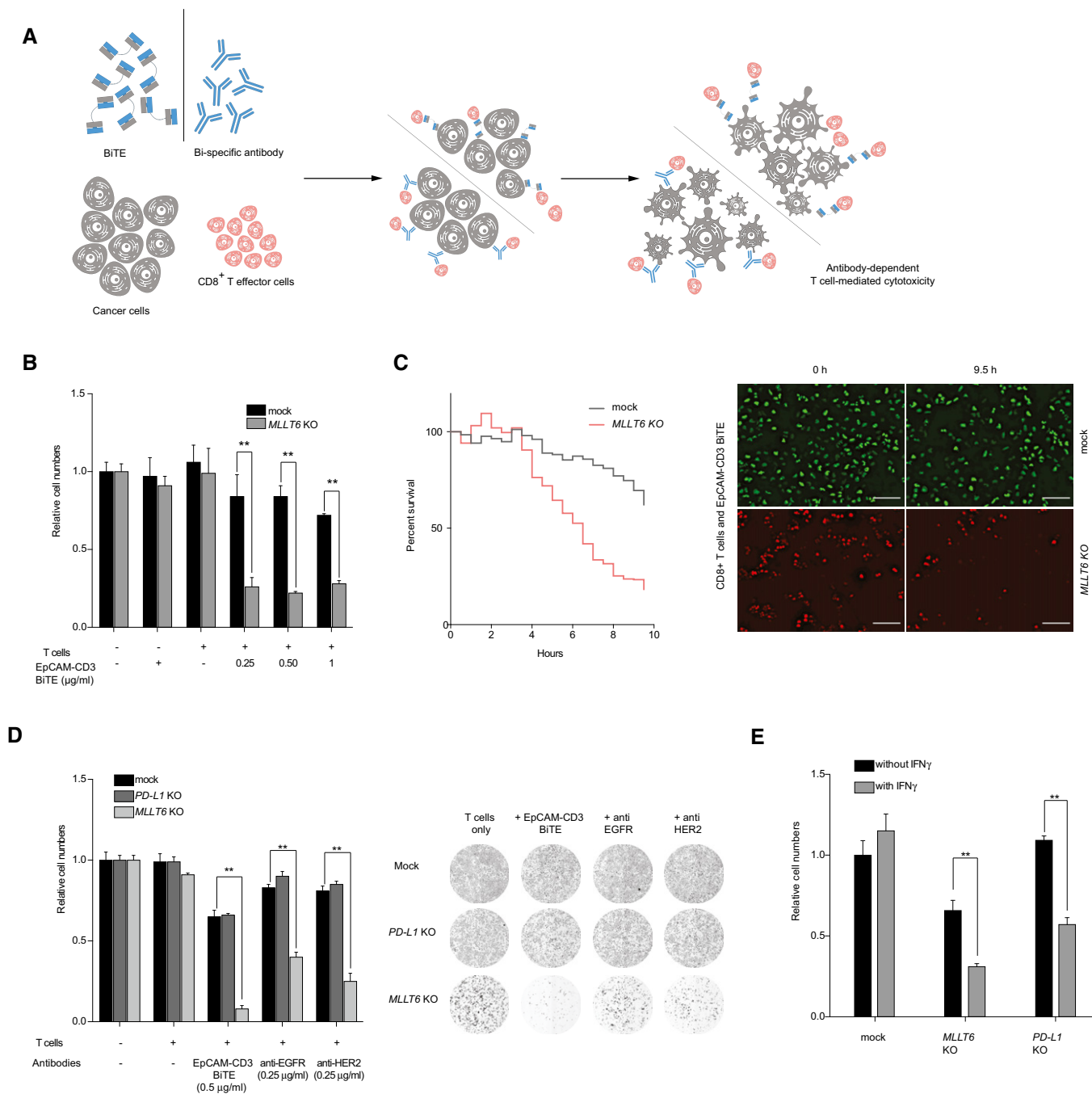
Figure 3. Knockout of *MLLT6* alleviates suppression of CTLs.

A Schematic of the assay measuring CD8$^+$ T cell-mediated cytotoxicity. Cancer cells (gray) with or without genetic modifications were mixed with BiTE or bi-specific antibodies with or without IFN-γ and cytotoxic T lymphocytes (CTLs). Altered tumor cell numbers were determined after allowing for T cell engagement.

B Relative cell numbers ($\pm$ SD; n = 3; biological replicates) of U2OS mock (black) or polyclonal *MLLT6* knockout (gray) cells treated with varying amounts of EpCAM-CD3 BiTE and CTLs (Student's t-test; **P < 0.01; degrees of freedom (df) = 4).

C Kaplan–Meier survival plot (left) showing changes in survival (percent) of mock (gray) and *MLLT6* knockout (red) cells treated with CTLs and EpCAM-CD3 BiTE over a course of 9.5 h. Representative images (right) of time-lapse fluorescence microscopy following U2OS mock (eGFP tagged, green) and *MLLT6* knockout (mCherry tagged, red) cells immediately (top left and bottom left) after adding CTLs and EpCAM-CD3 BiTE and 9.5 h later (top right and bottom right) (scale bars = 100 μm).

D Relative cell numbers (left) ($\pm$ SD; n = 3; biological replicates) of mock (black), *PD-L1* (dark gray) or *MLLT6* (light gray) knockout cells treated with BiTE or bi-specific antibodies and CTLs as indicated (Student's t-test; **P < 0.01; df = 4). Representative images (right) from bright field microscopy of polyclonal U2OS mock (top), *PD-L1* (middle) or *MLLT6* (bottom) knockout cells treated without or with EpCAM-CD3 BiTE or bi-specific antibodies.

E Relative normalized cell numbers ($\pm$ SD; n = 3; biological replicates) of U2OS mock (left), *MLLT6* (middle) or *PD-L1* (right) knockout cells treated with EpCAM-CD3 BiTE and CTLs in the presence (gray) or absence (black) of IFN-γ (Student's t-test; **P < 0.01; df = 4).

(Kiyozumi *et al*, 2018), *GBP5* (Tretina *et al*, 2019), *CXCL9* (Zhang *et al*, 2018), and *CXCL11* (Zhang *et al*, 2018) had well-known immune-related functions.

Next, we explored whether transcriptional changes observed in the RNA-Seq and NanoString experiments reflect on protein expression. To this end, we nominated five genes and quantified protein expression by immunoblotting in the presence and absence of *MLLT6* and IFN-γ (Fig 4C). We first determined whether protein levels increase upon IFN-γ stimulation in *MLLT6* wild-type cells (Fig 4C). In accordance with what was observed on transcript level, we found induction of *IDO1*, *HLA-DRB1*, *GBP5*, and *CD74* by IFN-γ. In sharp contrast, this induction was abolished in *MLLT6* knockout cells (Fig 4C). Collectively, these results establish *MLLT6* as a critical factor for IFN-γ signaling.

To further characterize the role of *MLLT6* in IFN-γ signaling, we examined the effects of MLLT6 depletion on members of the IFN-γ signal transduction pathway (Fig 5A). IFN-γ binds to two receptors (IFNGR1 and -2) that convey signals via Janus kinases 1 and 2 (JAK1 and JAK2), which in turn phosphorylate and activate STAT proteins (Zhang & Liu, 2017). Upon activation, STAT proteins dimerize and alter the expression of a series of interferon response genes (Zhang & Liu, 2017). To study changes in the components of the IFN-γ pathway, we first examined whether IFNGR1 and -2 expression differ upon *MLLT6* knockout and this may thereby explain the reduced sensitivity. We observed that expression of IFNGR1 and -2 was largely unaltered or even increased (IFNGR1: 2.9; IFNGR2: 1.4; Fig 5A). These results demonstrate that the observed insensitivity to IFN-γ stimulation after *MLLT6* knockout is not due to aberrant expression of IFNGRs. We then investigated changes in the components downstream of the IFN-γ receptor that mainly involve JAK/STAT proteins (Zhang & Liu, 2017). Immunoblotting did not show any significant differences in the levels of JAK1 or JAK2 expression in mock and *MLLT6* knockout samples treated with and without IFN-γ (Fig 5A). In contrast, a clear difference between *MLLT6* wild-type and knockout cells was observed for STAT1 (Fig 5A). While expression level of STAT1 is increased by IFN-γ stimulation in *MLLT6* knockout and wild-type cells, total levels stay lower in knockout cells (Fig 5A).

The *STAT1* gene encodes two isoforms, STAT1α and STAT1β, that are typically expressed conjointly (Zhang & Liu, 2017) and become phosphorylated upon activation (Zhang & Liu, 2017). Interestingly, it has been shown that the gene sets regulated by the two isoforms are not identical (Zakharova *et al*, 2003), and therefore, changes in the activation status of STAT1α or –β influence the transcriptional outcome. To investigate the activation status of STAT1 isoforms, we measured phosphorylation by immunoblotting. As reported in the literature (Zhang & Liu, 2017), we observed an induction of tyrosine 701 phosphorylation by IFN-γ (1.6) on both isoforms in wild-type cells. In contrast, loss of *MLLT6* expression resulted in a more pronounced STAT1β activation compared to STAT1α (Fig 5A) skewing the ratio between both isoforms. Although STAT1β is transcriptionally active in response to IFN-γ (Semper *et al*, 2014), it is considered the inhibitory form of STAT1 lacking most of the transactivation domain (Zakharova *et al*, 2003) and competes with STAT1α for binding to promoter regions (Zakharova *et al*, 2003; Baran-Marszak *et al*, 2004; Zhang & Liu, 2017). To validate the functional roles of the STAT1 isoforms in our cellular system, we specifically depleted STAT1α and STAT1β by
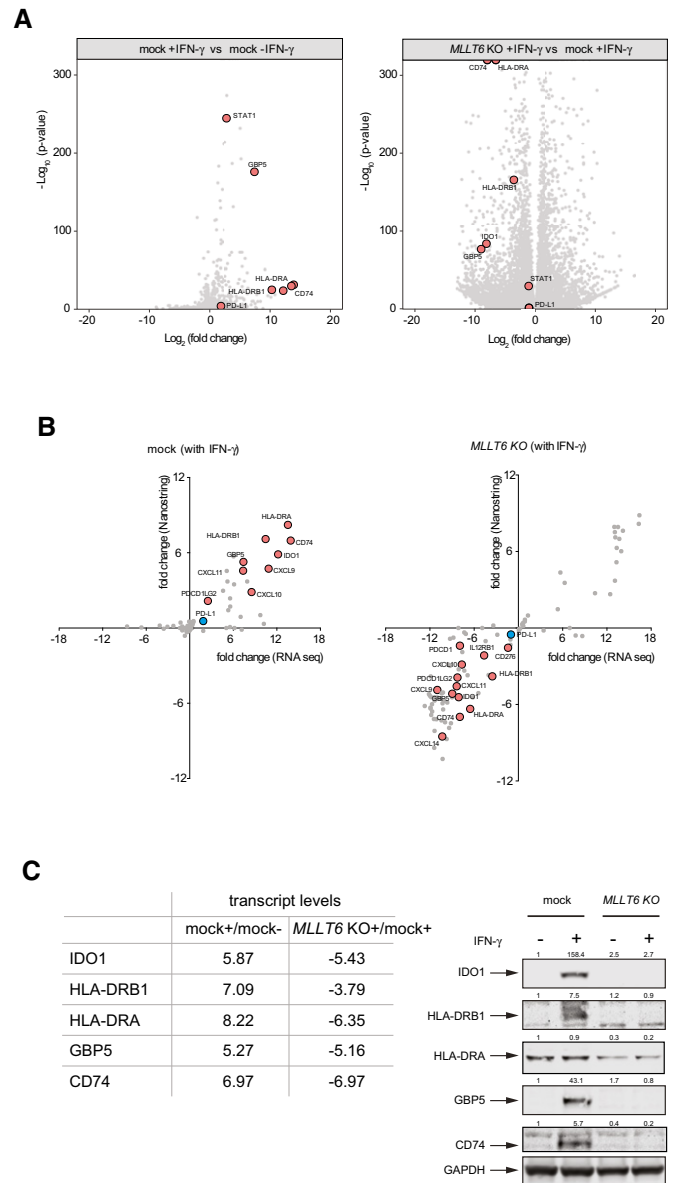

Figure 4. Role of *MLLT6* in gene expression.

A Scatter plots of pairwise comparisons of transcript expression in U2OS cells. Plots describe log$_2$ fold change in transcript expression in mock and polyclonal *MLLT6* knockout cells treated with and without IFN-γ as indicated. Horizontal axis shows log$_2$ fold change in transcript expression and vertical axis represents statistical significance (log$_{10}$ of *P*-value, *n* = 3) with candidates nominated for further validation (red).

B Correlation plots describing log$_2$ fold change of transcripts in RNA sequencing (*x*-axis) and NanoString (*y*-axis) measurements in mock cells ± IFN-γ (left) and *MLLT6* knockout cells with IFN-γ (right). Transcripts previously described to have a role in tumor immunity (red) and PD-L1 (blue) are represented on the plots as indicated.

C Changes (log$_2$ fold) in transcript expression (left) of select immune-related genes in U2OS mock or *MLLT6* knockout cells treated with or without IFN-γ and total protein levels measured by immunoblotting (right). Numbers indicate band intensities normalized to GAPDH.

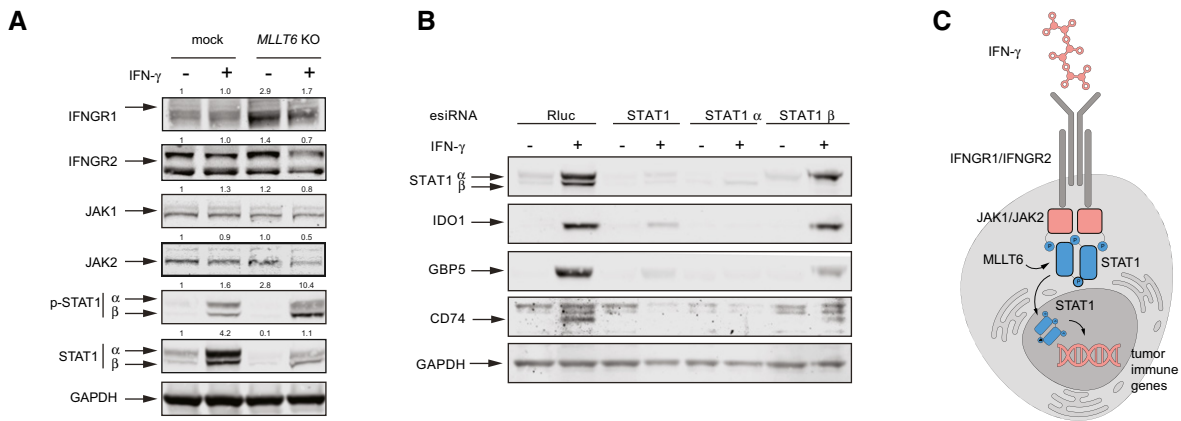Source data are available online for this figure.

Figure 5. Function of *MLLT6* in IFN-γ signaling.

A   Immunoblot expression analysis of proteins implicated in IFN-γ signal transduction in U2OS mock or polyclonal *MLLT6* knockout cells treated with or without IFN-γ. Numbers indicate band intensities normalized to GAPDH.

B   Immunoblot showing total protein levels of STAT1 isoforms (α and β), IDO1, GBP5, and CD74 in wild-type U2OS cells transfected with esiRNAs targeting Renilla luciferase (Rluc, negative control), total STAT1, STAT1α, and STAT1β treated with and without IFN-γ.

C   Schematic model of *MLLT6* function in IFN-γ signaling.

Source data are available online for this figure.

esiRNA-mediated RNAi (Kittler *et al*, 2007) (Fig 5B) and measured expression of *IDO1*, *GBP5*, and *CD74* before and after stimulation by IFN-γ. We observed that the depletion of STAT1β induced the expression of these three proteins, whereas knockdown of STAT1α downregulated their expression (Fig 5B). The data corroborate our model of STAT1 regulation by *MLLT6* (Fig 5C) and indicate a functional role of STAT1α as a transcriptional activator and of STAT1β as a transcriptional repressor. Hence, the observed differences in the phosphorylation of STAT1 isoforms in the absence of *MLLT6*, concomitantly with a general reduction in total *STAT1* expression level, may explain the reduced sensitivity to IFN-γ (Fig 5C).

Discussion

Harnessing the immune system has emerged as an important part of cancer therapy (Chen & Mellman, 2013). A prerequisite to this success has been the development of strategies that release the constraints of immune checkpoints (Ribas & Wolchok, 2018) and insights into the molecular regulation of essential checkpoint molecules offer unique opportunities for innovative therapies (Ribas & Wolchok, 2018). Our genetic CRISPR/Cas9 knockout screen, designed for enrichment of sgRNAs with high efficiency and phenotypic strength, identified previously unclassified genes implicated in cancer immune resistance. Although less suited for relative comparisons, the screen delivered genes implicated in the regulation of *PD-L1* expression. In particular, the screen identified the gene *MLLT6* as a regulator of factors required for tumor immune evasion. *Myeloid/lymphoid or mixed-lineage leukemia translocated to 6 (MLLT6)* encodes a protein containing a leucine zipper and a PHD finger motif both associated with transcriptional regulation (Prasad *et al*, 1994; Saha *et al*, 1995) and displays pronounced similarities to *MLLT10* (Marschalek, 2011). As observed with its paralog, a gene fusion of *MLLT6* to the histone H3 lysine 4 (H3K4)

methyltransferase *MLL* (*KMT2a*) has been reported in diverse cancer types (Prasad *et al*, 1994), including leukemia (Meyer *et al*, 2018; Chen *et al*, 2019). Myeloid/lymphoid or mixed-lineage leukemia (MLL) proteins are known to associate with DOT1L H3K79-methyltransferase (Bernt *et al*, 2011), a well-known epigenetic modifier controlling transcription of genes with strong implications in carcinogenesis (Bernt *et al*, 2011; Wang *et al*, 2016). While the molecular mechanism of the *MLL* gene in the fusion proteins in cancer transformation is well established (Marschalek, 2011), the role of the fusion partners is often less well understood. Our data suggest that *MLLT6* as a fusion partner might contribute to the transformation process by conveying a cancer immune editing strategy. Future work on cells harboring an *MLLT6-MLL* fusion could reveal if these cells are indeed compromised in immune checkpoint regulation.

T cell activation and inactivation requires the coordination of various costimulatory and coinhibitory signals (Ribas & Wolchok, 2018), and binding of PD-1 to its ligand PD-L1 is one such signal that negatively regulates the immune response (Sun *et al*, 2018). Unfortunately, the mechanisms governing immune escape in tumors are often similar, if not identical, to those governing self-tolerance (Sanmamed & Chen, 2018). Therefore, cancer patients receiving immune checkpoint inhibitors as part of their therapy exhibit immune-related adverse effects (irAEs; Mellati *et al*, 2015; Johnson *et al*, 2016). In addition, primary or acquired resistance to therapy provides a major challenge (Topalian *et al*, 2012; Ribas *et al*, 2016). Consequently, novel routes for tumor immune modulation are required. Our results demonstrate that depletion of MLLT6 in tumor cells alleviates suppression of T cell-mediated cytolysis and reduces expression of immune resistance factors. In gastric cancer, increased levels of MLLT6 correlates with a negative prognosis (Szasz *et al*, 2016), and in leukemia, activating mutations of *MLLT6* have been observed at a frequency higher than expected from random mutations (Meyer *et al*, 2018). Our

results suggest that these findings should be considered in light of MLLT6 as a regulator of tumor immune evasion. Furthermore, an *in vivo* RNAi screen in immune competent mice has recently identified *MLLT6* as a physiological regulator of oncogenic growth (Beronja *et al*, 2013). Our data indicate that *MLLT6* was identified in this screen due to its crucial role in cancer immune resistance. We speculate that Hras^{G12V} transformed cells lacking MLLT6 were eliminated by the host immune cells, while cells expressing *MLLT6* evaded the immune system and proliferated in this environment. Based on our results, we propose to re-examine the involvement of immune cells in this interesting *in vivo* system (Zhang *et al*, 2010; Beronja *et al*, 2013).

In addition to immunotherapies based on immune checkpoint blockade, other strategies evoking anti-cancer immunity have been developed, such as bi-specific antibodies (bsAbs) (Runcie *et al*, 2018) or BiTEs (Huehls *et al*, 2015). These molecules work by binding to T cell receptor (TCR) complex proteins such as CD3 and a common tumor antigen, thus engaging tumor and T cells (Huehls *et al*, 2015). Although these agents efficiently elicit an immune response against cancer cells *in vitro* (Deisting *et al*, 2015) and *in vivo* (Zhao *et al*, 2019), their clinical application is often limited due to the expression of immune repressors such as PD-L1 (Feucht *et al*, 2016) or IDO1 (Deisting *et al*, 2015). Our findings show that BiTE or bsAbs-mediated T cell cytolysis is augmented when *MLLT6* activity is inhibited. Hence, *MLLT6* inhibition can possibly reduce tumor-associated immune suppression and concurrently foster the efficacy of BiTEs or bsAbs. Therefore, a combination of *MLLT6* inhibition and T cell engagers is likely to improve clinical outcomes of therapy.

Besides oncogenic expression by cancer-associated signaling (Sharma *et al*, 2017), cytokine-induced immune resistance has also been reported (Zaidi & Merlino, 2011). IFN-γ is one such cytokine, typically secreted by lymphocytes, that convey both anti- and pro-tumorigenic signals (Zaidi & Merlino, 2011). IFN-γ plays an ambivalent role by stimulating the immune system but at the same time promoting factors that negatively affect the immune response (Garcia-Diaz *et al*, 2017). Its pronounced anti-tumorigenic activities include the upregulation of MHC class I molecules augmenting T-cell activation (Chang *et al*, 1992; Manguso *et al*, 2017), production of chemokines (Hu *et al*, 2008) recruiting immune effector cells (Pan *et al*, 2018) for eliminating tumor cells (Alspach *et al*, 2019). The loss of IFN-γ signaling reduces the efficacy of adoptive cell transfer and checkpoint blockade immunotherapy (Patel *et al*, 2017) but IFN-γ also promotes the development of regulatory T cells (Tregs) (Agnello *et al*, 2003) and upregulates the expression of *PD-L1* and *IDO1* to convey pro-tumorigenic effects (Zaidi & Merlino, 2011). Concomitantly, intratumoral IFN-γ was shown to be associated with expression of MHC class II molecules (Alspach *et al*, 2019), which in turn correlates with a more aggressive phenotype in human melanomas (Tsujisaki *et al*, 1987; Brocker *et al*, 1988; Hemon *et al*, 2011). Thus, a compelling interest in identifying modulators of IFN-γ signaling in tumors has emerged. Our data demonstrate that *MLLT6* is required for signal transduction of IFN-γ by modulating STAT1 activation. Although it is unclear whether such modulation occurs due to a direct or indirect interaction, our data show that loss of *MLLT6* in tumor cells reduces MHC class I expression in the presence of IFN-γ but induces the expression in

its absence, while MHC class II components are downregulated. However, the expression of the immunoproteasome components PSMB8 and PSMB9 reduces in *MLLT6* knockout cells and may therefore adversely affect MHC I peptide generation. Additionally, we show that *MLLT6* is required for IFN-γ stimulation of genes associated with immune evasion in tumor cells such as *IDO1, CD74,* and *GBP5.* Indoleamine 2,3-dioxygenase 1 (IDO1) is frequently found in the tumor microenvironment (Komiya & Huang, 2018), and high expression correlates with negative prognosis (Kiyozumi *et al*, 2018; Komiya & Huang, 2018). IDO1 expression leads to increased T cell anergy and enhanced Treg function (Komiya & Huang, 2018) increasing the capacity of tumors to attenuate immune response. Consequently, IDO1 inhibition alone or in combination with antibodies for PD-L1 is currently in clinical trials to enhance anti-tumor immunity (Komiya & Huang, 2018). CD74 is the invariant chain of the MHC class II complex and plays an important role in antigen presentation (Imaoka *et al*, 2019). Inhibition of CD74 signaling has been shown to restore anti-tumor immune response (Figueiredo *et al*, 2018) and reduce expression of PD-L1 (Imaoka *et al*, 2019), making it an interesting molecule for therapeutic targeting (Stein *et al*, 2007). Guanylate binding protein 5 (GBP5) belongs to a class of GTPases that have recently emerged as central orchestrators of host defense against a wide variety of pathogens and neoplastic diseases (Tretina *et al*, 2019). GBPs are induced by IFN-γ, and increased tissue levels have been found associated with unfavorable outcomes in lung adenocarcinoma (Yamakita *et al*, 2019). Based on our results tumor cells devoid of MLLT6 concomitantly lose expression of these proteins in the presence of IFN-γ, therefore, we speculate that the inhibition of MLLT6 may potentiate the effects of immunotherapies that invoke IFN-γ responses and thus boost their anti-tumorigenic effects. Additionally, combining MLLT6 inhibition with bsAbs, BiTEs or adoptive T cell therapies such as CAR T cells is conceivable.

Taken together, our data establish *MLLT6* as a regulator of immune-related genes that operate via the oncogenic and immune-associated signaling network. Although our conclusions are limited to bsAbs or BiTEs used *in vitro*, we are convinced that exploiting a tumor's dependency on *MLLT6* may open an alternative route to re-establish immune responses against cancer in patients resistant to current treatments.

Materials and Methods

Cell culture

The RKO, SW480 (colon carcinoma), HeLa (cervical carcinoma), and U2OS (osteosarcoma) cell lines were purchased from ATCC and maintained in DMEM (Gibco, ref: 31966-021) supplemented with 10% fetal bovine serum (Gibco, 10270-106) and 100 units/ml of penicillin and 0.1 mg/ml of streptomycin (Gibco, 15140-122) at 37°C and 5% CO_2. Whole blood samples were collected from four healthy donors in EDTA, and peripheral blood mononuclear cells (PBMCs) were isolated by density gradient centrifugation using Ficoll-Paque PLUS (GE Healthcare). Subsequently, CD8$^+$ T cells were subjected to negative selection using the CD8$^+$ T cell isolation kit (MACS, Miltenyi Biotec), expanded, and activated using

Dynabeads human T-Activator CD3/CD28 (Gibco) in ImmunoCult-XF T-cell expansion medium (Stemcell Technologies). Activation beads were removed after 72 h, and CD8$^+$ T cells were kept in culture for 24 h before functional tests were performed.

Reporter cell line

The RKO reporter cell line expressing PD-L1-eGFP was generated by homology-directed repair (HDR) after Cas9 cleavage of the genomic *PD-L1* locus. The HDR template was cloned into the vector pC-Goldy-TALEN (Addgene, 38143) via Esp3I containing an *eGFP-P2A-bsr* sequence flanked by 501 bp and 664 bp left and right homology arms, respectively (Fig EV1B). The HDR-vector was cotransfected with the vector pSpCas9(BB)-2A-Puro (PX459) V2.0 (Addgene, 62988) encoding *Streptococcus pyogenes* Cas9 and an sgRNA target-ing the genomic *PD-L1* locus close to the stop codon (gRNA PD-L1_HDR, 5′-GAGGAGACGTAATCCAGCAT-3′) by using Effectene (Qiagen) transfection reagent according to the manufacture's proto-col. After transfection, the cells were selected by blasticidin for HDR integration. Single cells with blasticidin resistance and eGFP fluores-cence were sorted by flow cytometry. Genomic DNA was extracted (QIAamp DNA blood kit, Qiagen) and probed for proper insertion of the reporter construct by PCR and Sanger sequencing (primers: P1, 5′-TCTCAGCAGGATCTGGAGCT-3′; P2, 5′-AGCTAAACAAGTTGCCCCC-3′; P3, 5′-TCTCAGCAGGATCTGGAGCT-3′; P4, 5′-ATTGTATTATAAAAGGACAGTGGGTGG-3′; P5, 5′-TGGAGAGGCACTAAGAGGGA-3′; P6, 5′-ACTTTTGATCAGTTTTCTGGCAAG-3′). For IFN-γ stimu-lation, cells were treated with varying amounts (0.5–50 ng/ml) of IFN-γ (BD PharMingen, 554617) in DMEM supplemented with 10% FBS, Pen/Strep and 2 mg/ml of bovine serum albumin (BSA) (Sigma-Aldrich, A7906) for 24 h. Media was then replaced with normal DMEM and various measurements were carried out.

CRISPR library

A sgRNA library was designed systematically to cover six protein classes, which include kinases, nuclear receptors, cell surface proteins (Bausch-Fluck *et al*, 2015), epigenetic factors, transcription factors, and uncharacterized genes. Genes with low expression (FPKM < 2) in RKO cells (Klijn *et al*, 2015) were excluded, and 3–7 different sgRNAs were designed to either target the first exon, an early splicing site or the functional domain of the protein. All sgRNAs were chosen to fulfill sequence features associated with high efficacy as previously described (Doench *et al*, 2016). The total library was composed of 10,722 sgRNA targeting 1,572 genes. 671 sgRNAs targeting control genes were divided into three categories: (i) 45 essential genes as general positive controls, (ii) assay controls, such as *PD-L1*, *eGFP*, or *STAT1*, and (iii) 47 non-essential genes as negative controls with no known function in PD-L1 signaling. Oligonucleotides with sgRNA sequences were ordered as arrayed synthesis (CustomArray Inc.) and PCR-amplified (primer, forward 5′-GATATTGCAACGTCTCACACC-3′, reverse 5′-GTCGCGTACGTCTCGAAAC-3′). The PCR product was cloned via Esp3I in the lentiviral vector pL.CRISPR.EFS.tRFP (#57819, Addgene) containing the modi-fied tracr sequence (5′-GTTTAAGAGCTATGCTGGAAACAGCATAG CAAGTTTAAATAAGGCTAGTCCGTTATCAACTTGAAAAAGTGGCA CCGAGTCGGTGCTTTTTTT-3′) as previously described (Chen *et al*, 2013).

Lentiviral production and CRISPR screen

Lentivirus was produced by transfection of HEK293T cells with the lentiviral vectors pL.CRISPR.EFS.tRFP (Addgene, 57818) and the packaging plasmids psPAX2 (Addgene, 12260) and pMD2.G (Addgene, 12259) at a mass ratio of 1.0:0.6:0.3. Transfection was performed using 45 μg polyethylenimine (Sigma-Aldrich) per 16 μg DNA. The supernatant containing the virus was collected 72 h after transfection, filtered through a 0.45-μm filter, diluted with cell culture medium in a ratio of 1:2, and added to the cells for 14 h incubation after centrifugation at 1,000 g for 30 min. For the screen, PD-L1-eGFP reporter cells were transduced with the sgRNA library at a multiplicity of infection of 0.15 with a tRFP expression vector that encodes for *Streptococcus pyogenes* Cas9 and sgRNA. Cells were subjected to FACS on a BD FACSAriaIII cell sorter, and 0.85×10^6 tRFP$^+$ cells were collected 5 days after infection. After sorting for tRFP$^+$ cells, they were incubated for 8 days and split into two flasks, which were left untreated or treated with 1.0 ng/ml IFN-γ for 48 h. Cells expressing low levels of PD-L1 were enriched by three rounds of FACS on a BD FACSAriaIII cell sorter 15, 27 and 41 days after lentiviral transduction (Fig EV2). Genomic DNA was extracted (QIAamp DNA blood kit, Qiagen) from unsorted cells 13 days post-transduction and after three rounds of sorting from sorted cells, 48 days post-transduction. sgRNA sequences were amplified by two rounds of PCR, with the second round primers containing adaptors for Illumina sequencing (PCR 1, forward 5′-GTAATAATTTCTTGGG TAGTTTGCA-3′, reverse 5′-ATTGTGGATGAATACTGCCATTTG-3′; PCR 2, forward 5′-ACACTCTTTCCCTACACGACGCTCTTCCGATCTG GCTTTATATATCTTGTGGAAAGG-3′, reverse 5′- GTGACTGGAGTT CAGACGTGTGCTCTTCCGATCTCAAGTTGATAACGGACTAGCC-3′). The resulting libraries were sequenced with single-end reads on a NextSeq 500. In brief, after targeted PCR amplification, the samples were indexed for NGS sequencing in a successive PCR enrichment followed by purification and capillary electrophoresis (Fragment Analyzer, Agilent). The sequence reads were mapped to sgRNA sequences with the aid of PatMaN (Prufer *et al*, 2008), a rapid short sequence aligner. As a set of query patterns, we used sgRNA sequences flanked by 5′-GACGAAACACCG-3′ and 5′-GTTTAA-GAGCTA-3′ on the termini, respectively, and allowed two mismatches during the alignment step. For each read, the best matching gRNA sequence was picked, and in case of ties, the read was discarded as ambiguous. Finally, for each sequenced sample, counts of reads mapped to each sgRNA from the library were calcu-lated.

CRISPR/Cas9 and BAC experiments

Synthetic oligonucleotides (Sigma-Aldrich) containing the sgRNA target site were phosphorylated, annealed, and cloned via BbsI into the vectors pSpCas9(BB)-2A-Puro (PX459) V2.0 (Addgene, 62988) or pSpCas9(BB)-2A-GFP (PX458) (Addgene, 48138). For CRISPR/Cas9-mediated gene disruption, RKO, SW480, HeLa, or U2OS cells were transfected with Cas9/sgRNA expression vectors using Invitro-gen Lipofectamine 2000 (Thermo Fisher Scientific, 11668019) or Fugene HD (Promega, E2311) and sorted for eGFP expression or selected by puromycin, respectively. RKO *MLLT6* knockout cells were identified after single cell sorting utilizing flow cytometry and genotyped. In brief, regions targeted by Cas9 were amplified by PCR

(primer, forward 5′-ATGAAGGAGATGGTAGGAGG-3′, reverse 5′-CGTGCCCATCGCAGTAGA-3′) and cloned into the vector pCR2.1 using the TA Cloning Kit (Thermo Fisher Scientific, 450046). *E. coli* strain DH5α was transformed with the TA cloned product, and single colonies were picked after blue-white screening for sequencing of the inserted PCR products. In case of U2OS, HeLa, and SW480 cells, a polyclonal *MLLT6* knockout line was created by flow cytometry analysis for cell surface PD-L1 (only U2OS) followed by PCR, TA cloning, and sequencing as described above. A bacterial artificial chromosome (BAC) harboring *MLLT6* genomic locus was obtained from Eupheria Biotech. The BAC contained a localization and affinity purification (LAP) cassette (Cheeseman & Desai, 2005) inserted as a carboxy-terminal fusion to *MLLT6*. Isolated BAC DNA was transfected and selected for stable integration as described (Poser *et al*, 2008).

esiRNA transfection

U2OS wild-type cells were seeded onto a six-well plate in DMEM supplemented with 10% FBS and Pen/Strep 24 h prior to transfection. 840 ng of various esiRNAs with 10 µl Oligofectamine diluted in OptiMEM were combined incubated at room temperature for 20 min and pipetted onto the cells. 48 h post-transfection, cells were treated with IFN-γ for another 24 h and subjected to protein extraction for Western blotting.

CTL assay

U2OS wild-type and *MLLT6* knockout cells were seeded onto a 96-well plate in DMEM supplemented with 10% FBS and Pen/Strep. After 24 h preactivated CD8$^+$ T cells, at varying ratios to cancer cells, in ImmunoCult-XF T Cell Expansion Medium with different amounts of EpCAM-CD3 BiTE or EGFR-CD3 or HER2-CD3 bi-specific antibodies were added onto control and knockout cells. Cells were incubated for 12–15 h and were fixed with 4% paraformaldehyde for 10 minutes at room temperature followed by washes with PBS and were subsequently permeabilized and stained with a mixture of 0.1% Triton X-100 (Serva, 37240) and 1 µg/ml of DAPI (AppliChem, A1001) in PBS for seven minutes at room temperature. Plates were subjected to fluorescent image based automated cell counting on a Celigo Imaging Cytometer (Nexcelom Bioscience). Statistical significance was determined using Student's two-tailed *t*-test by GraphPad Prism (version 6.04).

Time-lapse microscopy

U2OS wild-type and *MLLT6* knockout cells were transfected with pEGFP-C1 EGFP-3XNLS (Addgene, 58468) and pmCherry-C1 mCherry-NLS (Addgene, 58476) plasmids, respectively, to generate eGFP and mCherry expressing stable lines. A 50:50 mixture of 30,000 WT-eGFP and *MLLT6*-KO-mCherry cells were seeded into a µ-Slide 8 well-chambered coverslip slide (ibidi) containing 100 µl of DMEM supplemented with 10% FBS and Pen/Strep. The media was replaced with 300 µl of FluoroBrite DMEM (Gibco) containing T cells in the ratio of 3:1 to cancer cells and 0.2 µg of anti-EpCAM-CD3 bi-specific antibodies (Creative Biolabs). Time-lapse microscopy-based imaging was performed employing the Deltavision Elite deconvolution microscope. Images were acquired on FITC and

Alexa 594 channels every 10 min for 10 hours using a 20×/1.00 plan-Apochromat objective at 37°C with 5% CO$_2$. Subsequently, images were deconvolved and z-projected using image processing and analysis software, Fiji (Schindelin *et al*, 2012). Wild-type and *MLLT6* KO cell numbers were determined by manually counting cells on every image captured at 30-min intervals to generate a Kaplan–Meier curve.

Immunofluorescence

Cells were grown on coverslips overnight, fixed in methanol at −20°C for 10 min, quenched in acetone for 1 min, and blocked with 0.2% gelatin from cold-water fish skin (Sigma-Aldrich) in PBS (PBS/FSG) for 20 min. Cells were stained by incubation with primary antibodies for 1 h in PBS/FSG and washed with PBS/FSG. The cells were then incubated with fluorescent-dye conjugated secondary antibodies for 1 h at room temperature. After washing with PBS/FSG, coverslips were mounted on glass slides containing 4′,6-diamidino-2-phenylindole (DAPI; ProLong Gold anti-fade; Thermo Fisher Scientific). Images were acquired on an Olympus IX71 equipped with the DeltaVision Elite imaging system using 40×/0.95 plan apo objective, deconvolved, and projected using softWoRx software (Applied Precision). Acquired images were cropped and contrast adjusted using Fiji (Schindelin *et al*, 2012).

Antibodies

Immunofluorescence: goat anti-eGFP (MPI-CBG, Antibody Facility), mouse anti-α-tubulin (MPI-CBG, Antibody Facility), donkey anti-mouse Alexa594 (Thermo Fisher Scientific, 13497317), donkey anti-goat FITC (Thermo Fisher Scientific, 15343856). Flow cytometry: PE mouse IgG1, κ isotype control (BD PharMingen, 555749), PE mouse anti-human CD274 (BD PharMingen, 557924), FITC mouse anti-human EpCAM (BD PharMingen, 347197), FITC mouse IgG1, κ isotype control (BD PharMingen, 349041), APC anti-human EGFR antibody (BioLegend, 352906), APC mouse IgG1, κ isotype control (FC) antibody (BioLegend, 400122), PE anti-human EGFR antibody (BioLegend, 352903), PE mouse IgG1, κ isotype control (FC) antibody (BioLegend, 400113), FITC anti-human CD340 (erbB2/HER-2) antibody (BioLegend, 324404), FITC mouse IgG1, κ isotype control antibody (Biolegend, 400108). Western Blot: rabbit anti-PD-L1 (E1L3N) XP (Cell Signaling Technology, 13684), rabbit anti-PD-L1 (Thermo Fisher scientific, PA5-28115), goat anti-GAPDH (Acris Antibodies, AP16240PU-N), rabbit anti-IFNGR1 (Cell Signaling Technology, 34808), rabbit anti-IFNGR2, C-term (Gene Tex, GTX81601), rabbit anti-JAK1(6G4) (Cell Signaling Technology, 3344), rabbit anti-JAK2 (D2E12) (Cell Signaling Technology, 3230), rabbit anti-IDO1 (Gene Tex, GTX113753), rabbit anti-HLA-DRB1 (N1C3) (Gene Tex, GTX104919), rabbit anti-HLA-DRA (N2C3) (Gene Tex, GTX113732), rabbit anti-CD74 (Gene Tex, GTX110477), rabbit anti-GBP5 (Gene Tex, GTX106994), rabbit anti-STAT1 (Cell Signaling Technology, 9172), rabbit anti-phospho-STAT1 (Tyr701) (D4A7) (Cell Signaling Technology, 7649), IRDye 680LT donkey anti-goat IgG (LI-COR Biosciences, 926-68024), IRDye 800 CW donkey anti-rabbit IgG (LI-COR Biosciences, 926-32213). T cell activation: APC mouse anti-human CD3 (BD PharMingen, 555342), APC-Cy7 CD8 (BD PharMingen, 348813), PE-Cy7 mouse anti-human

CD25 (BD PharMingen 557741), FITC mouse anti-human CD69 (BD PharMingen, 557049). Bi-specific Antibodies: Recombinant anti-EpCAM-CD3 bi-specific T cell engagers were from Creative Biolabs (BITE-L022). Recombinant anti-HER2 x anti-CD3 and anti-EGFR x anti-CD3 tetravalent bi-specific (scFv-hIgG1Fc-scFv)$_2$ antibodies were cloned and produced by the DKFZ (Heidelberg).

Flow cytometry

Cells were trypsinized, and 250,000 cells were centrifuged at 2,000 g for 3 min and washed in PBS. Cells were stained with phycoerythrin (PE) mouse isotype control or PE mouse anti-PD-L1 antibody (1 µl in 100 µl PBS), FITC (fluorescein isothiocyanate) mouse IgG1, κ isotype control or FITC mouse anti-human EpCAM antibody (5 µl in 100 µl PBS), APC (allophycocyanin) mouse IgG1, κ isotype control or APC anti-human EGFR antibody, PE mouse IgG1, κ isotype control or PE anti-human EGFR antibody and FITC mouse IgG1, κ isotype control, or FITC anti-human CD340 (erbB2/HER-2) antibody (1 µl in 100 µl PBS) and incubated for 30 min at 4°C and 30 min at room temperature. Cells were then washed with PBS twice and resuspended in 250 µl of PBS and analyzed on BD FACSCalibur, Canto II or MACS Quant VYB flow cytometers. CD8$^+$ T cell activation status was confirmed by staining with antibodies against CD3, CD8, CD25, and CD69 (BD Pharmingen) followed by flow cytometry analysis on a BD LSR II flow cytometer. Statistical significance was determined using Student's two-tailed t-test by GraphPad Prism (version 6.04).

Western blotting

Protein extracts were prepared from RKO and U2OS cell lines by isolating four million cells washing with 500 µl PBS and treatment with 200 µl lysis buffer (280 mM NaCl, 0.5% Igepal, 5 mM MgCl$_2$-hexahydrate, 10% glycerol, and 50 mM Tris–HCl) containing Halt protease and phosphatase inhibitor cocktail (Thermo Fisher Scientific, 1861281) and 5 µl of 25 U/µl benzonase (Novagen, 70664) for 10 min on ice. Nine µl of samples was then mixed with 3 µl of 4× loading dye (62.5 mM Tris–HCl pH 6.8, 10% glycerol, 1% LDS, 0.005% bromophenol blue, and 50 mM DTT). Samples were then heated at 50°C for 5 min, centrifuged for 1 min at 18,400 g and loaded onto a NuPAGE 4–12% Bis-Tris protein gel (Invitrogen), electrophoresed and transferred to a nitrocellulose membrane. Subsequently, membranes were blocked in 5% non-fat dry milk, probed with indicated primary (overnight 4°C) and secondary (1 h at room temperature) antibodies and imaged on LI-COR Odyssey imaging system. Quantification of bands was performed using Image Studio Lite.

RNA sequencing

U2OS wild-type and *MLLT6* knockout lines were plated on 10 cm dishes for 24 h and then treated with 1.5 ng/ml of recombinant human IFN-γ and 20 mg/ml of bovine serum albumin for 24 h. RNA was isolated as per manufacturer's instructions using the RNeasy kit (Qiagen, 74104). Samples were run on an agarose gel to check RNA integrity, and 2 µg of total RNA from each sample was submitted for Illumina deep sequencing. Transcript expression levels were quantified with Salmon (Patro *et al*, 2017) using GENCODE release 28 (Patro *et al*, 2017) as a transcriptome annotation database. Differential expression analysis was performed in R (https://www.R-project.org, version 3.5) using tximport (Soneson *et al*, 2015) and DESeq2 (Love *et al*, 2014) packages.

NanoString

U2OS wild-type and *MLLT6* knockout cell lines treated with and without IFN-γ were subjected to RNA isolation as mentioned above. Samples were checked for RNA integrity, and 150 ng of total RNA was added to a master mix containing buffer, gene-specific pool of probes, reporter tags, and universal capture tags and hybridized at 67°C for 20 h. Gene-specific probes and reporter tags were designed by NanoString Technologies Inc. Sequences for the probes and tags are provided in the Dataset EV6. Samples were transferred to an nCounter cartridge and then loaded into the Prep Station for hybridization and immobilization onto the sample cartridge for 3 h. Subsequently, the cartridge was transferred to the nCounter digital analyzer for scanning immobilized fluorescent reporters. Quality checks and data analysis were performed on the nSolver software as per manufacturer's instructions.

sgRNA and esiRNA sequences

A list of the sgRNA and esiRNA sequences and target genes used for screening is provided in the Dataset EV1. The esiRNAs were purchased from Eupheria Biotech. The targeting regions of the sgRNAs used for validation and characterization were MLLT6_sgRNA-1, 5′-CTGCGTATGTTCGGACGAGA–3′; MLLT6_sgRNA-2, 5′-AGGCACGTACTGCAGCACGA-3′; MLLT6_sgRNA-3, 5′-GCCTCATGATCGCTTCAACA-3′; MLLT6_sgRNA-4, 5′-TCGACATCCATGGCGGTTAC-3′; negative control, 5′-GGCCAGCCGGCAATTCGC-3′.

qRT–PCR

Cells were trypsinized, and 1 million cells were isolated and subjected to RNA extraction using the RNeasy kit (Qiagen) as per manufacturer's protocol. Total RNA (2.5 µg) was annealed with oligo dT at 65°C for 5 minutes, and cDNA was synthesized using SuperScript III Reverse Transcriptase (Thermo Fisher Scientific, 18080085). Quantitative real-time PCR was performed using ABsolute QPCR Mix, Sybr Green, no-ROX (Thermo Fisher Scientific, AB1158). qPCR primers used: TBP, forward 5′-AGGTTAGAAGGCCTTGTGCTC-3′, reverse 5′-GGAGAACAATTCTGGGTTTGATCA-3′; MLLT6, forward 5′-GGTGCCTTCATTCCCCTTTG-3′, reverse 5′-GCAGGGGTGAGGTCTCCAGT-3′; PD-L1, forward 5′-TCATGACCTACTGGCATTTGC-3′, reverse 5′-TTGTCCAGATGACTTCGGCC-3′. Expression levels of genes were determined by $2^{-\Delta\Delta Ct}$ method; C_t values of gene of interest were normalized to respective TATA-box binding protein (TBP) transcript C_t values and normalized to control samples.

Statistical analysis

Statistical analysis was carried out with GraphPad Prism (version 6.04). Typically, for two-way comparison Student's two-tailed t-test (degree of freedom as indicated) was used. P-values of < 0.05 were considered significant. One-way ANOVA was employed to ascertain statistically significant differences between more than two groups.

Testing for differential expression of genes between RNA-Seq samples was performed using the standard workflow of R package DESeq2 (Love *et al*, 2014), with *P*-values calculated using a Wald test, followed by an FDR adjustment according to a Benjamini and Hochberg method. MFI values were calculated by building the arithmetic average of the fluorescence intensities.

Data availability

The DeepSeq data from this publication have been deposited to the NIH Gene Expression Omnibus (GEO) database and assigned the identifier GSE144484 (http://www.ncbi.nlm.nih.gov/geo/query/acc.cgi?acc=GSE144484).

Expanded View for this article is available online.

Author contributions
MT conceived and supervised the study. SS, MT, MD, MB, and CB designed, interpreted, and performed experiments. FB analyzed and interpreted data. MP-R analyzed data and designed sgRNAs. MT and SS wrote the manuscript. MM and FM designed and produced bi-specific antibodies.

Conflict of interest
The authors declare that they have no conflict of interest.

References

Agnello D, Lankford CS, Bream J, Morinobu A, Gadina M, O'Shea JJ, Frucht DM (2003) Cytokines and transcription factors that regulate T helper cell differentiation: new players and new insights. *J Clin Immunol* 23: 147−161

Alspach E, Lussier DM, Schreiber RD (2019) Interferon gamma and its important roles in promoting and inhibiting spontaneous and therapeutic cancer immunity. *Cold Spring Harb Perspect Biol* 11: a028480

Baran-Marszak F, Feuillard J, Najjar I, Le Clorennec C, Bechet JM, Dusanter-Fourt I, Bornkamm GW, Raphael M, Fagard R (2004) Differential roles of STAT1alpha and STAT1beta in fludarabine-induced cell cycle arrest and apoptosis in human B cells. *Blood* 104: 2475−2483

Bausch-Fluck D, Hofmann A, Bock T, Frei AP, Cerciello F, Jacobs A, Moest H, Omasits U, Gundry RL, Yoon C *et al* (2015) A mass spectrometric-derived cell surface protein atlas. *PLoS One* 10: e0121314

Bernt KM, Zhu N, Sinha AU, Vempati S, Faber J, Krivtsov AV, Feng Z, Punt N, Daigle A, Bullinger L *et al* (2011) MLL-rearranged leukemia is dependent on aberrant H3K79 methylation by DOT1L. *Cancer Cell* 20: 66−78

Beronja S, Janki P, Heller E, Lien WH, Keyes BE, Oshimori N, Fuchs E (2013) RNAi screens in mice identify physiological regulators of oncogenic growth. *Nature* 501: 185−190

Boku N (2014) HER2-positive gastric cancer. *Gastric Cancer* 17: 1−12

Brocker EB, Zwadlo G, Holzmann B, Macher E, Sorg C (1988) Inflammatory cell infiltrates in human melanoma at different stages of tumor progression. *Int J Cancer* 41: 562−567

Burr ML, Sparbier CE, Chan YC, Williamson JC, Woods K, Beavis PA, Lam EYN, Henderson MA, Bell CC, Stolzenburg S *et al* (2017) CMTM6 maintains the expression of PD-L1 and regulates anti-tumour immunity. *Nature* 549: 101−105

Casey SC, Tong L, Li Y, Do R, Walz S, Fitzgerald KN, Gouw AM, Baylot V, Gutgemann I, Eilers M *et al* (2016) MYC regulates the antitumor immune response through CD47 and PD-L1. *Science* 352: 227−231

Chang CH, Hammer J, Loh JE, Fodor WL, Flavell RA (1992) The activation of major histocompatibility complex class I genes by interferon regulatory factor-1 (IRF-1). *Immunogenetics* 35: 378−384

Cheeseman IM, Desai A (2005) A combined approach for the localization and tandem affinity purification of protein complexes from metazoans. *Sci STKE* 2005: pl1

Chen DS, Mellman I (2013) Oncology meets immunology: the cancer-immunity cycle. *Immunity* 39: 1−10

Chen B, Gilbert LA, Cimini BA, Schnitzbauer J, Zhang W, Li GW, Park J, Blackburn EH, Weissman JS, Qi LS *et al* (2013) Dynamic imaging of genomic loci in living human cells by an optimized CRISPR/Cas system. *Cell* 155: 1479−1491

Chen X, Wang F, Zhang Y, Wang M, Tian W, Teng W, Ma X, Guo L, Fang J, Zhang Y *et al* (2019) Panoramic view of common fusion genes in a large cohort of Chinese *de novo* acute myeloid leukemia patients. *Leuk Lymphoma* 60: 1071−1078

Deisting W, Raum T, Kufer P, Baeuerle PA, Munz M (2015) Impact of diverse immune evasion mechanisms of cancer cells on T cells engaged by EpCAM/CD3-bispecific antibody construct AMG 110. *PLoS One* 10: e0141669

Doench JG, Fusi N, Sullender M, Hegde M, Vaimberg EW, Donovan KF, Smith I, Tothova Z, Wilen C, Orchard R *et al* (2016) Optimized sgRNA design to maximize activity and minimize off-target effects of CRISPR-Cas9. *Nat Biotechnol* 34: 184−191

Evers B, Jastrzebski K, Heijmans JP, Grernrum W, Beijersbergen RL, Bernards R (2016) CRISPR knockout screening outperforms shRNA and CRISPRi in identifying essential genes. *Nat Biotechnol* 34: 631−633

Feucht J, Kayser S, Gorodezki D, Hamieh M, Doring M, Blaeschke F, Schlegel P, Bosmuller H, Quintanilla-Fend L, Ebinger M *et al* (2016) T-cell responses against CD19^{+} pediatric acute lymphoblastic leukemia mediated by bispecific T-cell engager (BiTE) are regulated contrarily by PD-L1 and CD80/CD86 on leukemic blasts. *Oncotarget* 7: 76902−76919

Figueiredo CR, Azevedo RA, Mousdell S, Resende-Lara PT, Ireland L, Santos A, Girola N, Cunha R, Schmid MC, Polonelli L *et al* (2018) Blockade of MIF-CD74 signalling on macrophages and dendritic cells restores the antitumour immune response against metastatic melanoma. *Front Immunol* 9: 1132

Garcia-Diaz A, Shin DS, Moreno BH, Saco J, Escuin-Ordinas H, Rodriguez GA, Zaretsky JM, Sun L, Hugo W, Wang X *et al* (2017) Interferon receptor signaling pathways regulating PD-L1 and PD-L2 expression. *Cell Rep* 19: 1189–1201

Gomes B, Driessens G, Bartlett D, Cai D, Cauwenberghs S, Crosignani S, Dalvie D, Denies S, Dillon CP, Fantin VR *et al* (2018) Characterization of the selective indoleamine 2,3-Dioxygenase-1 (IDO1) catalytic inhibitor EOS200271/PF-06840003 supports IDO1 as a critical resistance mechanism to PD-(L)1 blockade therapy. *Mol Cancer Ther* 17: 2530–2542

Goytain A, Ng T (2020) NanoString nCounter technology: high-throughput RNA validation. *Methods Mol Biol* 2079: 125–139

Green MR, Monti S, Rodig SJ, Juszczynski P, Currie T, O'Donnell E, Chapuy B, Takeyama K, Neuberg D, Golub TR *et al* (2010) Integrative analysis reveals selective 9p24.1 amplification, increased PD-1 ligand expression, and further induction via JAK2 in nodular sclerosing Hodgkin lymphoma and primary mediastinal large B-cell lymphoma. *Blood* 116: 3268–3277

Havel JJ, Chowell D, Chan TA (2019) The evolving landscape of biomarkers for checkpoint inhibitor immunotherapy. *Nat Rev Cancer* 19: 133–150

Hemon P, Jean-Louis F, Ramgolam K, Brignone C, Viguier M, Bachelez H, Triebel F, Charron D, Aoudjit F, Al-Daccak R *et al* (2011) MHC class II engagement by its ligand LAG-3 (CD223) contributes to melanoma resistance to apoptosis. *J Immunol* 186: 5173–5183

Hu X, Chakravarty SD, Ivashkiv LB (2008) Regulation of interferon and Toll-like receptor signaling during macrophage activation by opposing feedforward and feedback inhibition mechanisms. *Immunol Rev* 226: 41–56

Huehls AM, Coupet TA, Sentman CL (2015) Bispecific T-cell engagers for cancer immunotherapy. *Immunol Cell Biol* 93: 290–296

Ikeda S, Okamoto T, Okano S, Umemoto Y, Tagawa T, Morodomi Y, Kohno M, Shimamatsu S, Kitahara H, Suzuki Y *et al* (2016) PD-L1 is upregulated by simultaneous amplification of the PD-L1 and JAK2 genes in non-small cell lung cancer. *J Thorac Oncol* 11: 62–71

Imaoka M, Tanese K, Masugi Y, Hayashi M, Sakamoto M (2019) Macrophage migration inhibitory factor-CD74 interaction regulates the expression of programmed cell death ligand 1 in melanoma cells. *Cancer Sci* 110: 2273–2283

Johnson DB, Balko JM, Compton ML, Chalkias S, Gorham J, Xu Y, Hicks M, Puzanov I, Alexander MR, Bloomer TL *et al* (2016) Fulminant myocarditis with combination immune checkpoint blockade. *N Engl J Med* 375: 1749–1755

Kittler R, Surendranath V, Heninger AK, Slabicki M, Theis M, Putz G, Franke K, Caldarelli A, Grabner H, Kozak K *et al* (2007) Genome-wide resources of endoribonuclease-prepared short interfering RNAs for specific loss-of-function studies. *Nat Methods* 4: 337–344

Kiyozumi Y, Baba Y, Okadome K, Yagi T, Ishimoto T, Iwatsuki M, Miyamoto Y, Yoshida N, Watanabe M, Komohara Y *et al* (2018) IDO1 expression is associated with immune tolerance and poor prognosis in patients with surgically resected esophageal cancer. *Ann Surg* 269: 1101–1108

Klijn C, Durinck S, Stawiski EW, Haverty PM, Jiang Z, Liu H, Degenhardt J, Mayba O, Gnad F, Liu J *et al* (2015) A comprehensive transcriptional portrait of human cancer cell lines. *Nat Biotechnol* 33: 306–312

Komiya T, Huang CH (2018) Updates in the clinical development of epacadostat and other indoleamine 2,3-dioxygenase 1 inhibitors (IDO1) for human cancers. *Front Oncol* 8: 423

Kunz M, Toksoy A, Goebeler M, Engelhardt E, Brocker E, Gillitzer R (1999) Strong expression of the lymphoattractant C-X-C chemokine Mig is associated with heavy infiltration of T cells in human malignant melanoma. *J Pathol* 189: 552–558

Love MI, Huber W, Anders S (2014) Moderated estimation of fold change and dispersion for RNA-seq data with DESeq2. *Genome Biol* 15: 550

Manguso RT, Pope HW, Zimmer MD, Brown FD, Yates KB, Miller BC, Collins NB, Bi K, LaFleur MW, Juneja VR *et al* (2017) *In vivo* CRISPR screening identifies Ptpn2 as a cancer immunotherapy target. *Nature* 547: 413–418

Marschalek R (2011) Mechanisms of leukemogenesis by MLL fusion proteins. *Br J Haematol* 152: 141–154

Matern BM, Olieslagers TI, Voorter CEM, Groeneweg M, Tilanus MGJ (2019) Insights into the polymorphism in HLA-DRA and its evolutionary relationship with HLA haplotypes. *HLA* 95: 117–127

Mellati M, Eaton KD, Brooks-Worrell BM, Hagopian WA, Martins R, Palmer JP, Hirsch IB (2015) Anti-PD-1 and Anti-PDL-1 monoclonal antibodies causing type 1 diabetes. *Diabetes Care* 38: e137–e138

Meyer C, Burmeister T, Groger D, Tsaur G, Fechina L, Renneville A, Sutton R, Venn NC, Emerenciano M, Pombo-de-Oliveira MS *et al* (2018) The MLL recombinome of acute leukemias in 2017. *Leukemia* 32: 273–284

Mezzadra R, Sun C, Jae LT, Gomez-Eerland R, de Vries E, Wu W, Logtenberg MEW, Slagter M, Rozeman EA, Hofland I *et al* (2017) Identification of CMTM6 and CMTM4 as PD-L1 protein regulators. *Nature* 549: 106–110

Ni L, Lu J (2018) Interferon gamma in cancer immunotherapy. *Cancer Med* 7: 4509–4516

Pan D, Kobayashi A, Jiang P, Ferrari de Andrade L, Tay RE, Luoma AM, Tsoucas D, Qiu X, Lim K, Rao P *et al* (2018) A major chromatin regulator determines resistance of tumor cells to T cell-mediated killing. *Science* 359: 770–775

Parsa AT, Waldron JS, Panner A, Crane CA, Parney IF, Barry JJ, Cachola KE, Murray JC, Tihan T, Jensen MC *et al* (2007) Loss of tumor suppressor PTEN function increases B7-H1 expression and immunoresistance in glioma. *Nat Med* 13: 84–88

Patel SJ, Sanjana NE, Kishton RJ, Eidizadeh A, Vodnala SK, Cam M, Gartner JJ, Jia L, Steinberg SM, Yamamoto TN *et al* (2017) Identification of essential genes for cancer immunotherapy. *Nature* 548: 537–542

Patro R, Duggal G, Love MI, Irizarry RA, Kingsford C (2017) Salmon provides fast and bias-aware quantification of transcript expression. *Nat Methods* 14: 417–419

Poser I, Sarov M, Hutchins JR, Heriche JK, Toyoda Y, Pozniakovsky A, Weigl D, Nitzsche A, Hegemann B, Bird AW *et al* (2008) BAC TransgeneOmics: a high-throughput method for exploration of protein function in mammals. *Nat Methods* 5: 409–415

Prasad R, Leshkowitz D, Gu Y, Alder H, Nakamura T, Saito H, Huebner K, Berger R, Croce CM, Canaani E (1994) Leucine-zipper dimerization motif encoded by the AF17 gene fused to ALL-1 (MLL) in acute leukemia. *Proc Natl Acad Sci USA* 91: 8107–8111

Prufer K, Stenzel U, Dannemann M, Green RE, Lachmann M, Kelso J (2008) PatMaN: rapid alignment of short sequences to large databases. *Bioinformatics* 24: 1530–1531

Ribas A, Hamid O, Daud A, Hodi FS, Wolchok JD, Kefford R, Joshua AM, Patnaik A, Hwu WJ, Weber JS *et al* (2016) Association of pembrolizumab with tumor response and survival among patients with advanced melanoma. *JAMA* 315: 1600–1609

Ribas A, Wolchok JD (2018) Cancer immunotherapy using checkpoint blockade. *Science* 359: 1350–1355

Runcie K, Budman DR, John V, Seetharamu N (2018) Bi-specific and tri-specific antibodies- the next big thing in solid tumor therapeutics. *Mol Med* 24: 50

Saha V, Chaplin T, Gregorini A, Ayton P, Young BD (1995) The leukemia-associated-protein (LAP) domain, a cysteine-rich motif, is present in a

wide range of proteins, including MLL, AF10, and MLLT6 proteins. *Proc Natl Acad Sci USA* 92: 9737−9741

Sanmamed MF, Chen L (2018) A paradigm shift in cancer immunotherapy: from enhancement to normalization. *Cell* 175: 313−326

Schindelin J, Arganda-Carreras I, Frise E, Kaynig V, Longair M, Pietzsch T, Preibisch S, Rueden C, Saalfeld S, Schmid B *et al* (2012) Fiji: an open-source platform for biological-image analysis. *Nat Methods* 9: 676−682

Seliger B, Ruiz-Cabello F, Garrido F (2008) IFN inducibility of major histocompatibility antigens in tumors. *Adv Cancer Res* 101: 249−276

Semper C, Leitner NR, Lassnig C, Parrini M, Mahlakoiv T, Rammerstorfer M, Lorenz K, Rigler D, Muller S, Kolbe T *et al* (2014) STAT1beta is not dominant negative and is capable of contributing to gamma interferon-dependent innate immunity. *Mol Cell Biol* 34: 2235−2248

Sharma P, Hu-Lieskovan S, Wargo JA, Ribas A (2017) Primary, adaptive, and acquired resistance to cancer immunotherapy. *Cell* 168: 707−723

Soneson C, Love MI, Robinson MD (2015) Differential analyses for RNA-seq: transcript-level estimates improve gene-level inferences. *F1000Res* 4: 1521

Stein R, Mattes MJ, Cardillo TM, Hansen HJ, Chang CH, Burton J, Govindan S, Goldenberg DM (2007) CD74: a new candidate target for the immunotherapy of B-cell neoplasms. *Clin Cancer Res* 13: 5556s−5563s

Sun C, Mezzadra R, Schumacher TN (2018) Regulation and function of the PD-L1 checkpoint. *Immunity* 48: 434−452

Szasz AM, Lanczky A, Nagy A, Forster S, Hark K, Green JE, Boussioutas A, Busuttil R, Szabo A, Gyorffy B (2016) Cross-validation of survival associated biomarkers in gastric cancer using transcriptomic data of 1,065 patients. *Oncotarget* 7: 49322−49333

Topalian SL, Hodi FS, Brahmer JR, Gettinger SN, Smith DC, McDermott DF, Powderly JD, Carvajal RD, Sosman JA, Atkins MB *et al* (2012) Safety, activity, and immune correlates of anti-PD-1 antibody in cancer. *N Engl J Med* 366: 2443−2454

Tretina K, Park ES, Maminska A, MacMicking JD (2019) Interferon-induced guanylate-binding proteins: Guardians of host defense in health and disease. *J Exp Med* 216: 482−500

Tsujisaki M, Igarashi M, Sakaguchi K, Eisinger M, Herlyn M, Ferrone S (1987) Immunochemical and functional analysis of HLA class II antigens induced by recombinant immune interferon on normal epidermal melanocytes. *J Immunol* 138: 1310−1316

Wang X, Chen CW, Armstrong SA (2016) The role of DOT1L in the maintenance of leukemia gene expression. *Curr Opin Genet Dev* 36: 68−72

Wieser V, Gaugg I, Fleischer M, Shivalingaiah G, Wenzel S, Sprung S, Lax SF, Zeimet AG, Fiegl H, Marth C (2018) BRCA1/2 and TP53 mutation status associates with PD-1 and PD-L1 expression in ovarian cancer. *Oncotarget* 9: 17501−17511

Yamakita I, Mimae T, Tsutani Y, Miyata Y, Ito A, Okada M (2019) Guanylate binding protein 1 (GBP-1) promotes cell motility and invasiveness of lung adenocarcinoma. *Biochem Biophys Res Commun* 518: 266−272

Zaidi MR, Merlino G (2011) The two faces of interferon-gamma in cancer. *Clin Cancer Res* 17: 6118−6124

Zakharova N, Lymar ES, Yang E, Malik S, Zhang JJ, Roeder RG, Darnell JE Jr (2003) Distinct transcriptional activation functions of STAT1alpha and STAT1beta on DNA and chromatin templates. *J Biol Chem* 278: 43067−43073

Zhang Z, Huang L, Reisenauer MR, Wu H, Chen L, Zhang Y, Xia Y, Zhang W (2010) Widely expressed Af17 is likely not required for embryogenesis, hematopoiesis, and animal survival. *Genesis* 48: 693−706

Zhang Y, Liu Z (2017) STAT1 in cancer: friend or foe? *Discov Med* 24: 19−29

Zhang C, Li Z, Xu L, Che X, Wen T, Fan Y, Li C, Wang S, Cheng Y, Wang X *et al* (2018) CXCL9/10/11, a regulator of PD-L1 expression in gastric cancer. *BMC Cancer* 18: 462

Zhao J, Song Y, Liu D (2019) Recent advances on blinatumomab for acute lymphoblastic leukemia. *Exp Hematol Oncol* 8: 28

Zhu H, Bengsch F, Svoronos N, Rutkowski MR, Bitler BG, Allegrezza MJ, Yokoyama Y, Kossenkov AV, Bradner JE, Conejo-Garcia JR *et al* (2016) BET bromodomain inhibition promotes anti-tumor immunity by suppressing PD-L1 expression. *Cell Rep* 16: 2829−2837